Clays and Clay Minerals, Vol. 52, No. 1, 106–114, 2004.

FORMATION OF NONTRONITE FROM OXIDATIVE DISSOLUTION OF PYRITE DISSEMINATED IN PRECAMBRIAN FELSIC METAVOLCANICS OF THE SOUTHERN IBERIAN MASSIF (SPAIN)

J. C. Fernández-Caliani[1,*], E. Crespo[2], M. Rodas[2], J. F. Barrenechea[2] and F. J. Luque[2]

[1] Departamento de Geología, Facultad de Ciencias Experimentales, Universidad de Huelva, 21071 Huelva, Spain
[2] Departamento de Cristalografía y Mineralogía, Facultad de Geología, Universidad Complutense de Madrid, 28040 Madrid, Spain

Abstract—This paper describes a rare occurrence of nontronite associated with sulfide-bearing felsic metavolcanics, providing evidence of colloidal deposition in open spaces as result of a low-temperature water-rock interaction. Microbotryoidal masses of green nontronite with impurities of kaolinite, illite, barite, amorphous silica and iron oxyhydroxides are found as vein and cavity fillings in deeply kaolinized rhyolites and rhyolitic tuffs of Precambrian age, at Oliva de Mérida in SW Spain. Clay mineral characterization has been carried out by X-ray diffraction, infrared spectroscopy, thermal analysis, analytical electron microscopy and stable isotope (oxygen and hydrogen) analysis. Nontronite was formed under low-temperature alteration conditions, from a continuous sequence of reactions and aqueous solution compositions, involving two basic processes that acted in concert: oxidative dissolution of pyrite and hydrolysis of K-feldspar. After acidity neutralization, dissolved silica released by incongruent dissolution of K-feldspar reacted with ferric sulfate derived from pyrite oxidation to form nontronite under oxidizing conditions, in the presence of relatively warm meteoric water.

Key Words—Felsic Metavolcanics, K-feldspar Hydrolysis, Nontronite, Pyrite Oxidation, Smectite, Spain, Weathering.

INTRODUCTION

Nontronite is a 2:1 swelling phyllosilicate in which tetrahedral sites are predominantly occupied by Si cations, but some replacement of Si by Al and Fe^{3+} can occur, whereas most of the octahedral sites are filled by Fe^{3+} (>1.0 cation per half unit-cell according to Güven, 1988), with minor amounts of Al. Thus, the general structural formula for nontronite can be written as follows: $M_{x+y}[Si_{8-x-y}Al_xFe^{3+}_y][Fe^{3+}_{4-z}Al_z]O_{20}(OH)_4{\cdot}nH_2O$, where M refers to exchangeable interlayer cations. Nontronite is regarded, therefore, as the ferric end-member of dioctahedral smectites. Details on its structure and crystal chemistry are given in Güven (1988) and references therein.

Although nontronite has been studied extensively, it continues to attract a high level of research interest, especially for interplanetary life. Indeed, this ferric smectite is relevant to the search for life on planets like Mars, owing to its high Fe content and because it can be a potential source of water (Frost *et al.*, 2002).

In terrestrial environments nontronite is not abundant. However, it is common in both oceanic and continental environments and often occurs as an authigenic clay mineral in recent submarine sediments, formed by direct precipitation from hydrothermal fluids discharged from active sea-floor spreading centres (Keeling *et al.*, 2000). For instance, it is a typical clay mineral of deep-sea sediments from marine white smoker chimneys of the Red Sea, Galapagos rift, Mariana trough, and Juan de Fuca ridge, among other hydrothermal systems (Cole and Shaw, 1983; Murnane and Clague, 1983; Singer *et al.*, 1984; Singer and Stoffers, 1987; Köhler *et al.*, 1994). In this oceanic environment, nontronite occurs not only near hydrothermal vent openings, but also on the sea-floor by alteration of glassy balsaltic lava flows, as well as microbially-mediated low-temperature reaction of iron oxyhydroxides with silica (Juniper and Tebo, 1995; Ueshima and Tazaki, 2001).

Under supergene conditions, nontronite is a common weathering product of basalts and ultramafic rocks (*e.g.* Bender-Koch *et al.*, 1995). It is also found in highly weathered metamorphic rocks, such as schists, gneisses and amphibolites (Keeling *et al.*, 2000). Moreover, it has been reported in felsic volcanics either as an alteration product of Fe-rich silicates (Shenk and Armbruster, 1985), or around rootless fumaroles by leaching and dissolution of rhyolitic ignimbrites (Reyes and Read, 2002).

In this paper we describe a new occurrence of nontronite in Spain which is associated with sulfide-bearing felsic volcano-sedimentary rocks. We suggest a model of nontronite formation in these exotic parent rocks based on mineralogical and geochemical data, together with field and petrographic observations.

* E-mail address of corresponding author:
caliani@uhu.es
DOI: 10.1346/CCMN.2004.0520110

GEOLOGICAL SETTING

Nontronite occurrences are located near Oliva de Mérida, ~20 km to the SE from the roman city of Mérida, in the province of Badajoz (SW Spain). From a geological standpoint, the mineralization is found in association with a volcano-sedimentary sequence of Middle-Upper Riphean age (Figure 1), at the Precambrian basement of the Ossa-Morena Zone, in the SW margin of the Iberian Massif (Gibbons and Moreno, 2002).

The volcano-sedimentary sequence is a succession of predominantly felsic metavolcanics (volumetrically, rhyolites are the most abundant) and volcanoclastic rocks (mainly rhyolitic tuffs and tuffaceous shales) interbedded with metasediments (schists, quartzites and pelitic gneisses), mafic metavolcanics and amphibolites. Volcanic-hosted disseminated pyrite appears within the volcano-sedimentary package, in close spatial relationship to the felsic rocks. Supergene weathering oxidized the sulfides forming numerous goethite concretions and abundant ferruginous surface coatings.

According to IGME (1988), the Precambrian materials constitute the core of the Oliva de Mérida anticlinorium, and form part of the Tentudía-Montemolín series (Eguiluz *et al.*, 1984), belonging to the Alange Unit of the Obejo-Valsequillo-Puebla de la Reina domain. All these rocks were affected by Cadomian tectonothermal events (Quesada, 1990) and later they were deformed and metamorphosed during the Variscan orogeny.

MATERIALS AND ANALYTICAL METHODS

A cm-scale grid was used to collect clayey samples from the outcrop examined in the field (section A-B in Figure 1). In addition, a series of representative samples of the host rocks was collected for petrographic analysis.

Mineralogical characterization was performed using a combination of analytical methods including transmitted-light optical microscopy, X-ray diffraction (XRD), Fourier transform infrared spectroscopy (FTIR), differential thermal and thermogravimetric analysis (DTA-TGA), scanning electron microscopy (SEM), energy dispersive X-ray spectroscopy (EDS), and stable isotope (oxygen and hydrogen) analysis.

X-ray diffraction was used to determine the bulk composition of the samples, after gentle grinding and

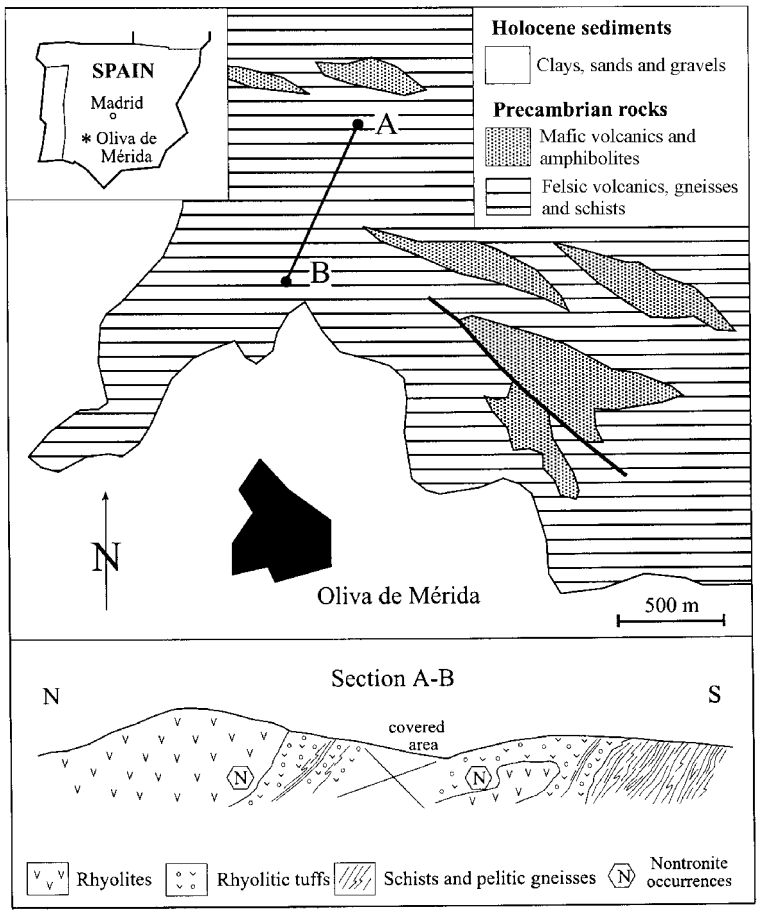

Figure 1. Generalized geological map of the Oliva de Mérida area depicting a section with the nontronite occurrences within a volcano-sedimentary sequence of Middle–Upper Riphean age.

https://doi.org/10.1346/CCMN.2004.0520110 Published online by Cambridge University Press

homogenization to <53 μm. For clay mineral identification, carefully hand-picked samples were disaggregated in an ultrasonic bath. From these samples, oriented aggregates of the <2 μm size fraction were obtained by sedimentation from an aqueous suspension, pipetted onto glass slides and dried. The oriented films were solvated with ethylene glycol and subjected to thermal treatment at 550ºC for 2 h (Moore and Reynolds, 1997). The XRD patterns of random powders and oriented aggregates were collected using Ni-filtered CuKα radiation with a Siemens D500 powder diffractometer equipped with a graphite monochromator. The XRD patterns were recorded with a microcomputer using the Siemens SOCABIM Diffract AT3.3 software.

The IR absorbance spectra were recorded in the middle IR region (spectral range between 400 and 4000 cm^{-1}) on a Nicolet, 20SXC FTIR spectrometer, using pressed pellets containing 3 mg of sample and 300 mg KBr. The DTA-TGA curves were obtained with a Seiko 320U instrument operating at a heating rate constant of, 20ºC/min, from ambient temperature (25ºC) to 1000ºC, in a static air atmosphere.

Fragments of each sample were mounted on stubs, coated with carbon, and examined by SEM in secondary electron mode in a Jeol JSM-5410 microscope, operated at an accelerating voltage of 15 kV. Quantitative chemical analyses were obtained by means of an Oxford Link system energy dispersive X-ray (EDS) analyzer coupled to the microscope.

The isotopic analyses were performed at the Stable Isotope Laboratory of Salamanca University, using a SIRA series II spectrometer from VG Isotech. Oxygen was extracted following Clayton and Mayeda's (1963) technique by reaction with ClF_3 (Borthwick and Harmon, 1982). Hydrogen was extracted following the procedures of Godfrey (1962).

FIELD AND PETROGRAPHIC RELATIONSHIPS

The nontronite occurrences display a clear epigenetic relationship to porphyritic felsic rocks containing phenocrysts of quartz and K-feldspar (sanidine) enclosed in a glassy groundmass, often showing perlitic cracks. Subordinate amounts of sodic plagioclase, muscovite and rutile are also present, and numerous scattered crystals of oxidized pyrite occur locally in the rhyolitic matrix (Figure 2a). The felsic volcanics are embedded within a volcano-sedimentary framework in which fine-grained rhyolitic tuffs and a sequence of predominantly sulfide-bearing black schists and quartzites can be distinguished. Likewise, all these rocks show field and petrographic evidence of extensive sulfide oxidization, such as veins and bands of mixed iron oxy-hydroxides and hematite pseudomorphous after pyrite crystals (Figure 3).

Bright apple green clayey material with a massive appearance occurs together with dendritic aggregates of iron oxyhydroxides as surface coatings along the sides of fissures (Figure 2b). Most of the mineralized fractures are oriented subvertically following the regional fracturing trend (mainly N50ºE and N135ºE). Furthermore, small masses of green clay, up to several dm thick, are found as veins, patches and cavity fillings in deeply kaolinized rhyolitic tuffs (Figure 2c). These felsic rocks are the main host to the mineralization, although the distribution of minerals is controlled by fracturing.

GENERAL CHARACTERIZATION

XRD

The green clays are composed of virtually pure smectite (Figure 4). The patterns of the oriented

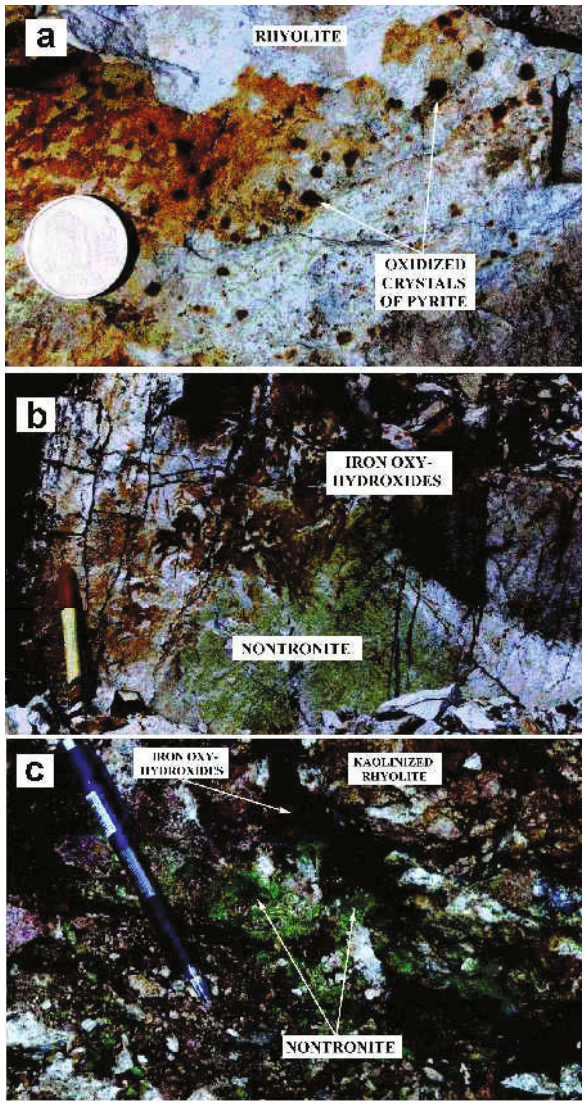

Figure 2. Field evidence of iron-sulfide oxidation in rhyolite (a) and types of occurrences of the greenish nontronite: (b) nontronite and iron oxy-hydroxidescoating fissure surfaces in rhyolite; (c) massive nontronite infilling cavities in highly kaolinized rhyolite.

https://doi.org/10.1346/CCMN.2004.0520110 Published online by Cambridge University Press

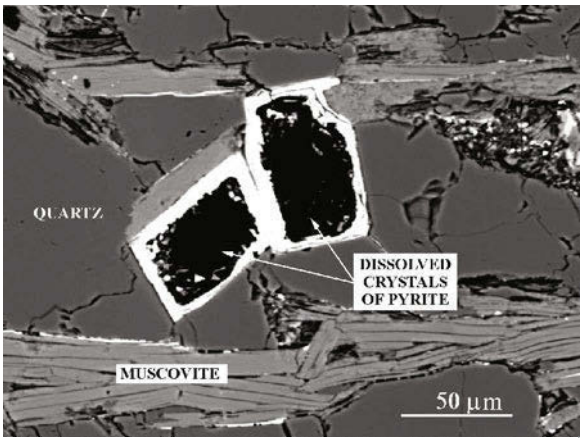

Figure 3. SEM-BSE image showing dissolved crystals of pyrite partially replaced by hematite in quartz-schist.

aggregates are similar and show a sharp and strong 001 reflection at ~14 Å in the air-dried mounts that shifted to ~16.6 Å after ethylene glycol solvation, and to ~9.6 Å after heating at 550ºC, indicating the presence of a highly crystalline smectite (Biscaye index = 0.954–0.992). The smectite contains a double layer of water molecules and exchangeable divalent cations in the interlayer space.

The b_0 parameter values (9.048–9.096 Å) derived from the position of the 060 reflection in the non-oriented powder XRD patterns are within the dioctahedral range of smectites. Brigatti (1983) and Köster *et al.* (1999) observed a linear correlation between the *b* unit-cell dimension of dioctahedral smectites and the total

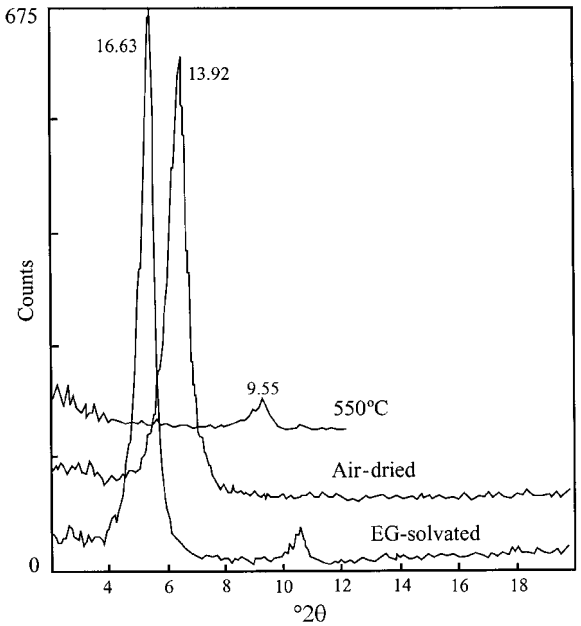

Figure 4. Typical XRD patterns for the oriented clay fraction of the Oliva de Mérida nontronite.

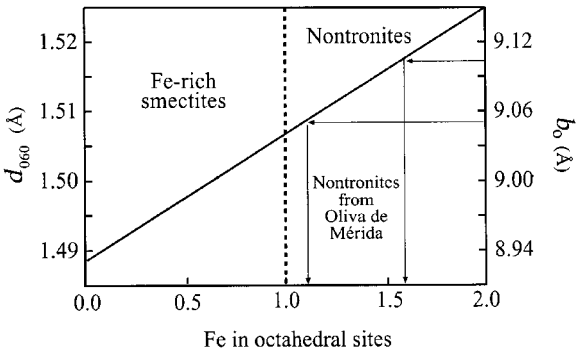

Figure 5. Nontronite *b* unit-cell dimension as measured by XRD *vs.* octahedral Fe content. Regression line established by Brigatti (1983).

number of Fe^{3+} ions in octahedral sites. Accordingly, the measured b_0 values plotted on the line of regression fitted in Figure 5, are consistent with an octahedral Fe content >1.0 atom per half unit-cell. The smectite can be regarded, therefore, as a true nontronite on the basis of Güven's (1988) classification scheme for dioctahedral smectites.

Infrared spectral analysis

A typical IR absorbance spectrum of the nontronite (Figure 6) is characterized by two broad bands in the OH-stretching region, centered at ~3560 and 3420 cm^{-1}. The first absorption band is attributed to Fe^{3+}–OH–Fe^{3+} vibrations indicating an Fe-rich smectite while the second is typically due to water (Petit *et al.*, 2002). A strong Si–O stretching band appears at 1021 cm^{-1}. The position of this band reflects little or no sustitution of Si by Fe^{3+} in the tetrahedral sheets (Goodman *et al.*, 1976). In the OH-bending region, three weak bands were observed at 864, 814 and 678 cm^{-1}, which can be assigned to the $Fe^{3+}Fe^{3+}$(OH) unit of nontronite (Russell and Fraser, 1994; Koster *et al.*, 1999).

Thermal analysis

The DTA-TGA pattern shown in Figure 7 illustrates the thermal decomposition of a typical nontronite

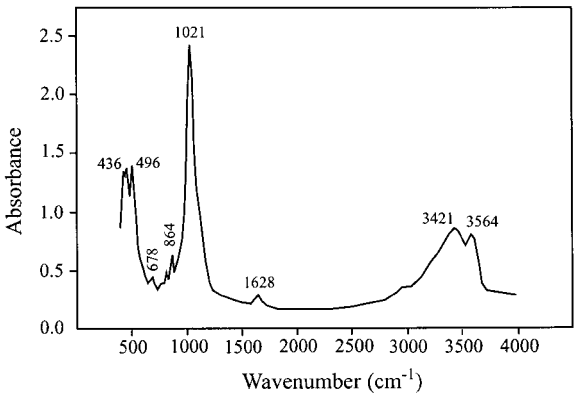

Figure 6. IR spectrum of Oliva de Mérida nontronite.

https://doi.org/10.1346/CCMN.2004.0520110 Published online by Cambridge University Press

sample. The first endothermic peak was observed at 90ºC, and it is attributed to the loss of adsorbed water. As a result of the water desorption, a loss of 13.4% in weight occurred. The dehydroxylation endothermic effect took place at 470ºC, and the weight loss during the dehydroxylation process was 5%. The analyses show that the nontronite from Oliva de Mérida has a thermal behavior similar to, but less complex than, nontronite described at other localities (Ding and Frost, 2002), although the less complex pattern could be a consequence of different heating ratios. For instance, Ding and Frost (2002) carried out the controlled rate thermal analysis operating at much slower heating rate (2ºC), thus obtaining two overlapping dehydroxylation steps.

The observed dehydroxylation temperature is consistent with the measured *b* unit-cell dimension (Figure 8), and also with the Fe content inferred by XRD, according to the regression equation given by Brigatti (1983).

Analytical scanning electron microscopy

The SEM images (Figure 9) show that massive nontronite is generally formed by microcrystalline aggregates consisting of lath-shaped crystals that often split into fine fiber-like particles (Figure 9a). Ribbons and delicate filaments of nontronite were also observed. The most conspicuous feature is the occurrence of globular or spherulitic aggregates forming a microbotryoidal texture (Figure 9b). The spherulites (150–200 μm in diameter) are made up of fibrous nontronite crystals (up to 100 μm in length) radiating from a common core.

Although the nontronite samples are nearly monomineralic, some ancillary phases were identified by SEM-EDS, such as kaolinite, which usually occurs as lath-like particles within the core of the spherulites (Figure 9c), mica, quartz, feldspars, poorly crystalline iron oxy-hydroxides, amorphous silica and clustered euhedral crystals of barite (Figure 9d).

In order to approximate the chemical composition of the smectite, chemical analyses by EDS were obtained from selected individual particles. The number of ions was calculated on the basis of 24 anions per formula from the weight percentages of the major constituent oxides, which were obtained by converting the X-ray spectrum to a quantitative analysis, making appropriate corrections (quantitative method ZAF). The results confirmed the nontronitic character of the smectites the number of measured Fe^{3+} ions being ~1.5 per half unit-cell. Nevertheless, taking into account the Fe/Fe+Al+Mg ratio (Figure 10), as derived from the number of ions calculation, significant compositional variations can be inferred within the ferric member of the beidellite–nontronite series. Minor amounts of Ca (<1 wt.% CaO), as detected by SEM-EDS, are present as exchangeable cation in the interlayer space, as previously deduced by XRD.

Stable isotope analysis

The stable isotope ratios of hydrogen (D/H) and oxygen ($^{16}O/^{18}O$) of a representative nontronite sample are −85.7 and +16.3‰, respectively, relative to SMOW. It can be assumed that nontronite has retained its original isotopic composition because no post-formational process is evident from field and petrographic relations. As shown in Figure 11, the δD value plotted against the δO value depicts a point in the supergene field (on the right of the S/H line), close to the kaolinite line, thus indicating that the nontronite mineralization was formed in equilibrium with meteoric waters (Sheppard and Gilg, 1996).

Clay minerals in low-temperature environments record the δD and δO values and temperature of the waters from which they formed because isotopic exchange rates are very slow (Kyser, 1987).

The oxygen isotope composition of water with which nontronite formed under equilibrium conditions can be calculated from the following equation, derived by Delgado and Reyes (1996):

$$\delta O_{water} = -19.25 + 0.125\delta D_{sm} + (12.33\delta O_{sm} - 1.54\delta D_{sm} + 252.2)^{1/2}$$

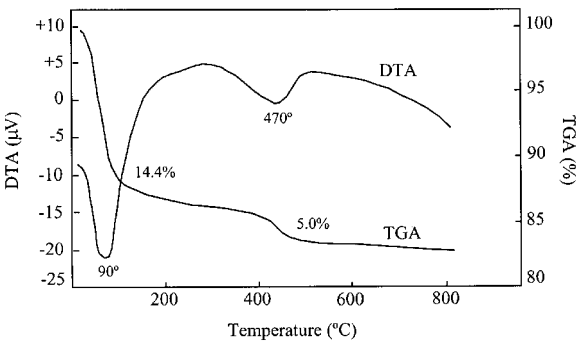

Figure 7. DTA-TGA diagram showing the endothermic reactions and weight loss found for the Oliva de Mérida nontronite.

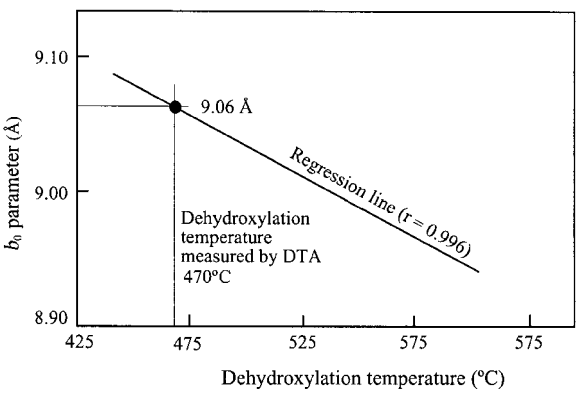

Figure 8. Dehydroxylation temperature of nontronite as determined by DTA *vs. b* unit-cell dimension. Regression equation proposed by Brigatti (1983).

https://doi.org/10.1346/CCMN.2004.0520110 Published online by Cambridge University Press

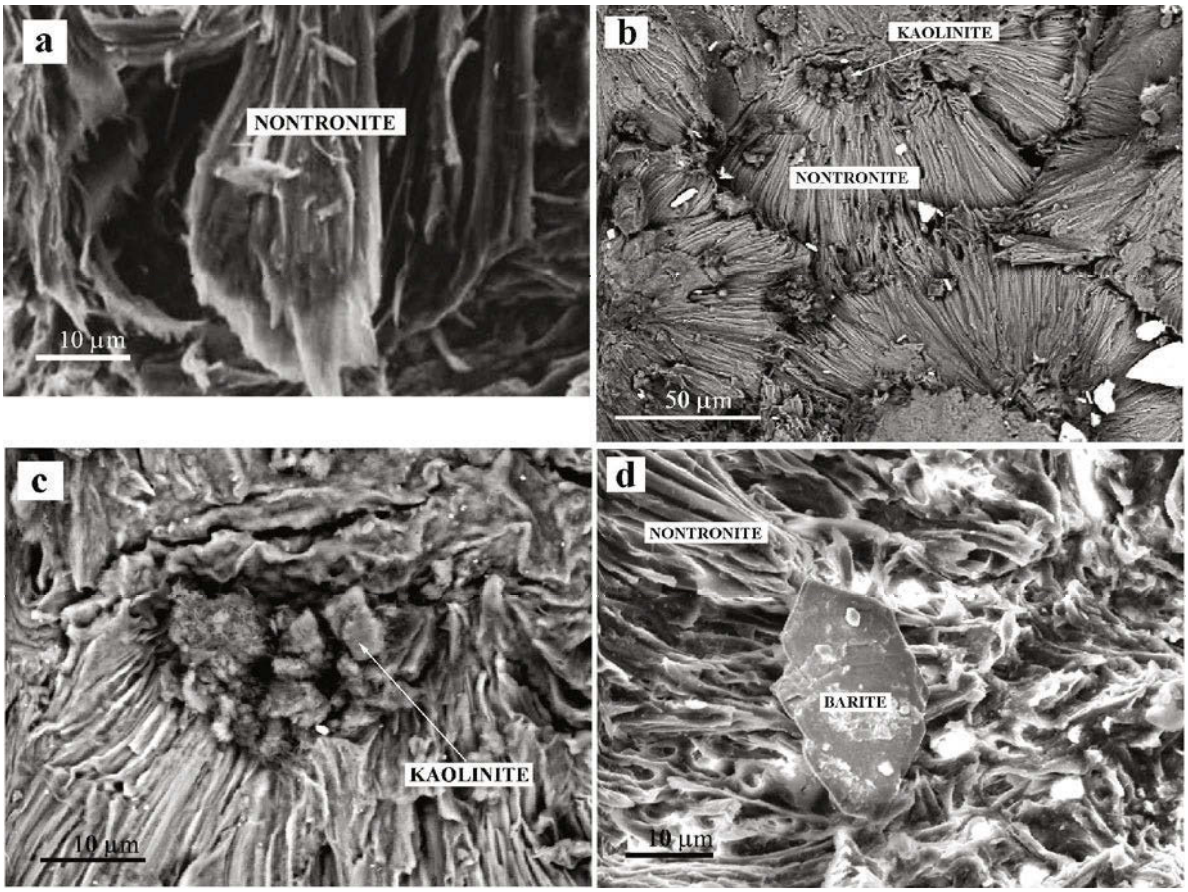

Figure 9. SEM-BSE images of nontronite samples showing: (a) lath-shaped crystals splitting into fine fiber-like morphologies; (b) spherulitic aggregates forming a microbotryoidal texture; (c) kaolinite pockets within the spherulites; (d) euhedral crystals of barite disseminated in the nontronite clays.

In this case, the δO value obtained for the water is −4.9‰. Taking into account that hydrogen and oxygen isotope compositions of the meteoric water are correlated by means of the global meteoric water line equation (Craig, 1961):

$$\delta D = 8\delta O + 10$$

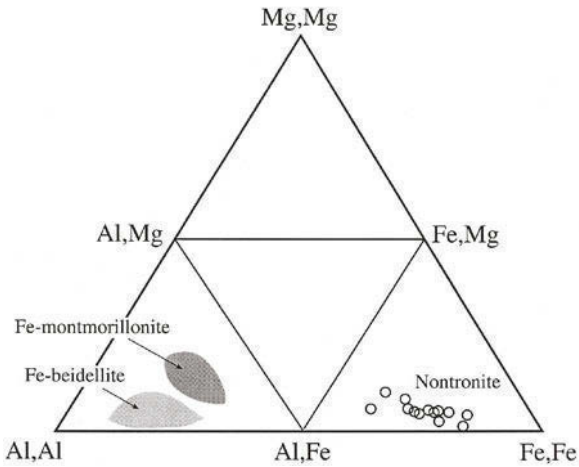

Figure 10. Projection on smectite compositional diagram (Güven, 1988) of the atomic proportions of Fe, Al and Mg obtained from selected chemical analyses performed by SEM-EDS on individual nontronite crystals.

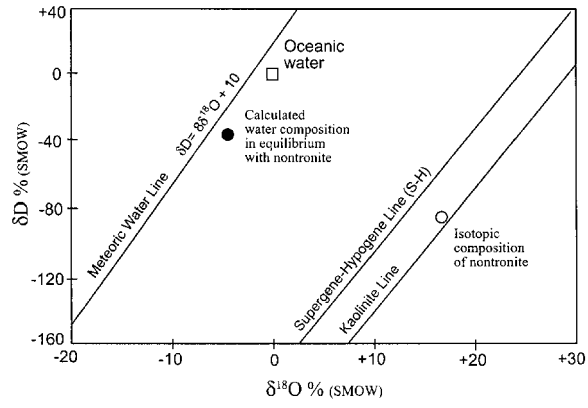

Figure 11. Hydrogen and oxygen isotope ratios of a representative nontronite sample and calculated isotope composition of water in equilibrium with nontronite. The meteoric water line (Craig, 1961), kaolinite weathering line (Savin and Epstein, 1970) and supergene/hypogene (S/H) line are given for reference.

https://doi.org/10.1346/CCMN.2004.0520110 Published online by Cambridge University Press

the δD value calculated for the water is −29.2‰. The results are in the range of those of the present-day rainwater values (Alley and Cuffey, 2001).

Lastly, in order to constrain the temperature of nontronite formation, we have used the equation derived by Delgado and Reyes (1996) for smectite which originated in open systems with high water-rock ratios and relatively low temperatures:

$$3.54 \times 10^6 T^{-2} = \delta O_{sm} - 0.125\delta D_{sm} + 8.95$$

thus obtaining a temperature of ~40ºC. Accordingly, the nontronite mineralization was formed from the weathering of the felsic metavolcanics under low-temperature alteration conditions. The age of weathering is uncertain because the Precambrian basement in SW Spain has been exposed to surface conditions since Late Carboniferous times.

NONTRONITE FORMATION

Three basic stages can be proposed in the nontronite formation process: (1) oxidation of pyrite and generation of acidic waters; (2) hydrolysis of K-feldspar and acid neutralization, and (3) precipitation of nontronite.

Stage I: oxidative dissolution of pyrite and acid generation

Oxidative dissolution of the pyrite hosted in the felsic metavolcanics and black schists took place during the weathering in the presence of meteoric water and excess of free oxygen, through the reaction:

$$2FeS_2 + 7O_2 + 2H_2O = 2Fe^{2+} + 4SO_4^{2-} + 4H^+ \qquad (1)$$

producing acid (two moles of H^+ by oxidation of one mole of pyrite) and leading to an increase in the chemical activities of S and Fe species in the aqueous solution. Because of the lowering of pH, Fe^{2+} was oxidized to Fe^{3+} according to the reaction:

$$Fe^{2+} + ¼O_2 + H^+ = Fe^{3+} + ½H_2O \qquad (2)$$

thus accelerating the pyrite oxidation rate because ferric Fe replaces oxygen as an oxidizing agent. In fact, the observed pyrite oxidation rate in the laboratory ranges between 1.08×10^{-15} and 1.8×10^{-14} mol cm^{-2} s^{-1}, but these rates can be increased by about 100 times in the presence of ferric iron in solution (Nicholson, 1994).

An assesment of acid generation of the sulfide-bearing felsic rocks can be made following Paktunc's (1999) approach:

$$AP = \frac{N_s W_a X_s}{W_s} \times 10$$

where AP is the acid potential of rocks, N_s is the number of moles of sulfuric acid formed by the oxidation of 1 mole of pyrite, W_a is the molecular weight of sulfuric acid, W_s is the molecular weight of pyrite, and X_s is the percentage of pyrite in the rocks. Considering that the felsic metavolcanics contain 5% of pyrite on average, the acid potential was ~82 kg of sulfuric acid equivalents per ton, which represent the volume of acid produced by the pyrite oxidation.

Stage II: hydrolysis of alkali feldspar and acid neutralization

As mentioned previously, the masses of nontronite are found in deeply kaolinized rhyolites and rhyolitic tuffs suggesting that hydrolysis of K-feldspar occurred as result of acid rock drainage. For simplicity, the water-rock interaction process can be described by incongruent dissolution of the K-feldspar to form kaolinite under acidic conditions, via the reaction:

$$2KAlSi_3O_8 + H_2SO_4 + 9H_2O = Al_2Si_2O_5(OH)_4 + 4H_4SiO_4 + 2K^+ + SO_4^{2-} \qquad (3)$$

More silica is present in the K-feldspar structure than is needed to form kaolinite, therefore some silica remains dissolved in the aqueous solution, together with K and sulfate ions.

Although the dissolution kinetics of K-feldspar are very slow (Blum and Stillings, 1995), the hydrolysis reaction consumed acid and became an important neutralization mechanism of the acidic water (two moles of K-feldspar were necessary to neutralize one mole of sulfuric acid). Despite their long-term buffering capacity, the felsic metavolcanics were alkaline enough to neutralize the acidity of the solutions, as determined on the basis of the net neutralizing potential (Paktunc, 1999).

The neutralizing potential (NP) can be calculated by:

$$NP = \frac{W a X_i}{N_i W_i} \times 10$$

where W_a is the molecular weight of sulfuric acid, X_i is the percentage of K-feldspar in the felsic rocks, N_i is the number of moles of K-feldspar required to consume one mole of sulfuric acid, and W_i is the molecular weight of the K-feldspar. Assuming that K-feldspar is by far the most abundant neutralizing phase in the felsic metavolcanics (60% on average), the bulk neutralizing potential calculated with this approach is ~105 kg of sulfuric acid equivalent per ton.

Since the net neutralization potential (NNP), *i.e.* the balance between NP and AP, is positive (NNP = 105−82 = 23 kg/ton), it can be concluded that the acidic solution was neutralized by the dissolution of the K-feldspar.

Stage III: precipitation of nontronite

The combined reaction of acid generation by pyrite oxidation and neutralization of the acidic solution by K-feldspar dissolution promoted a suitable environment for nontronite formation.

The major chemical species dissolved in the acidic aqueous solution from the above reactions were Fe^{3+}, K^+, SO_4^{2-} and silica. After acidity neutralization, the dissolved silica reacted with ferric sulfate derived from

https://doi.org/10.1346/CCMN.2004.0520110 Published online by Cambridge University Press

the pyrite oxidation to form nontronite under oxidizing conditions. This reaction can be written as follows:

$$2(SO_4)_3Fe_2 + 8SiO_2 + 8H_2O = Fe_4Si_8O_{20}(OH)_4 + 6H_2SO_4 \quad (4)$$

Significant concentrations of Al^{3+} may be dissolved in acidic (pH <4) aqueous solutions during the weathering (*e.g.* Huang and Keller, 1972). It can be assumed therefore that some of the Al^{3+} dissolved in the acidic aqueous solution was incorporated in the nontronite after acidity neutralization.

The volume of nontronite mineralization was controlled by the abundance of pyrite originally contained in the felsic rocks, and the extent of K-feldspar dissolution. The dissolution rate of the feldspar presumably determined the rate of the overall nontronite formation process.

It must be emphasized that nontronite started to precipitate once the acidic water was neutralized. Harder (1976) demonstrated from laboratory synthesis experiments that nontronite precipitation is achieved at surface temperatures with a pH >6. Similarly, accompanying phases such as Fe oxyhydroxides, amorphous silica and illite were formed by way of the following reactions:

$$Fe^{3+} + 2H_2O = FeOOH + 3H^+ \quad (5)$$

$$H_4SiO_4 = SiO_2 \text{ (amorphous silica)} + 2H_2O \quad (6)$$

$$K^+ + 3Al^{3+} + 3H_4SiO_4 = KAl_3Si_3O_{10}(OH)_2 + 10H^+ \quad (7)$$

With respect to the occurrence of authigenic barite in the green clays, since Ba is a common minor element in the K-feldspar structure (e.g. Deer *et al*., 1992), it can be readily explained by reaction of dissolved sulfate with Ba ions released into solution from the feldspar hydrolysis.

The colloform texture suggests that nontronite was deposited in fissures and open spaces, as a colloidal gel from a percolating supersaturated fluid, and it developed into larger and more ordered crystals with time. Hence, the structural discontinuities and other discrete pathflows of the felsic rock acted as channelways for relatively warm meteoric water along fault zones. The formation temperature (~40ºC) suggested by oxygen isotope composition is consistent with that of other nontronites formed under low-temperature alteration conditions (<70ºC) in both continental and oceanic environments (Köster *et al*., 1999).

The above genetic interpretation is based not only on the field, mineralogical and geochemical data presented here, but it is also supported by the experimental results of Decarreau *et al.* (1987) and Mizutani *et al.* (1991) who synthesized nontronite from silica gels and iron sulfate under oxidizing conditions.

CONCLUSIONS

The Precambrian sulfide-bearing felsic metavolcanics of the Oliva de Mérida underwent a low-temperature water-rock interaction process, resulting in complete oxidation of pyrite and subsequent precipitation of nontronite through a sequence of reaction products and aqueous solution compositions. The nontronite formation process can be summarized as follows: (1) production of acidic aqueous solution from interaction of meteoric water with sulfide-bearing felsic rocks; (2) dissolution of K-feldspar under the influx of acidic waters, release of cations and acidity neutralization; (3) nontronite precipitation through fissures of the felsic metavocanics from dissolved components in solution, after acidity neutralization.

ACKNOWLEDGMENTS

We thank R. Rojas and M.A. Muro from the Instituto de Ciencia de Materiales (CSIC) of Madrid for their technical assistance with the FTIR and DTA-TGA analyses. We wish to thank also Prof. Ray Ferrell and Dr David Patrick for their helpful comments.

REFERENCES

Alley, R.B. and Cuffey, K.M. (2001) Oxygen and hydrogen isotopic ratios of water in precipitation: Beyond Paleothermometry. Pp. 527–553 in: *Stable Isotope Geochemistry* (J.W. Valley and D.R. Cole, editors). Reviews in Mineralogy and Geochemistry, **43**. Mineralogical Society of America, Washington, D.C.

Bender-Koch, C., Morup, S., Madsen, M.B. and Vistisen, L. (1995) Iron-containing weathering products of basalt in a cold, dry climate. *Chemical Geology*, **122**, 109–119.

Blum, A.E. and Stillings, L.L. (1995) Feldspar dissolution kinetics. Pp. 291–351 in: *Chemical Weathering Rates of Silicate Minerals* (A.F. White and S.L. Brantley, editors). Reviews in Mineralogy, **31**. Mineralogical Society of America, Washington, D.C.

Borthwick, J. and Harmon, R.S. (1982) A note regarding ClF_3 as an alternative to BrF_5 for oxygen isotope analysis. *Geochimica et Cosmochimica Acta*, **46**, 1665–1668.

Brigatti, M.F. (1983) Relationships between composition and structure in Fe-rich smectites. *Clay Minerals*, **18**, 177–186.

Clayton, R.N. and Mayeda, T.D. (1963) The use of bromine pentafluoride in the extraction of oxygen from oxides and silicates for isotopic analysis. *Geochimica et Cosmochimica Acta*, **27**, 43–52.

Cole, T.G. and Shaw, H.F. (1983) The nature and origin of authigenic smectites in some recent marine sediments. *Clay Minerals*, **18**, 239–252.

Craig, H. (1961) Isotopic variations in meteoric waters. *Science*, **133**, 1702–1703.

Decarreau, A., Bonnin, D., Badaut-Trauth, D., Couty, R. and Kaiser, P. (1987) Synthesis and crystallogenesis of ferric smectite by evolution of Si-Fe coprecipitates in oxidizing conditions. *Clay Minerals*, **22**, 207–223.

Deer, W.A., Howie, R.A. and Zussman, J. (1992) *An Introduction to the Rock-Forming Minerals*, 2nd edition. Longmans, Essex, UK

Delgado, A. and Reyes, E. (1996) Oxygen and hydrogen isotope compositions in clay minerals: A potential single-mineral geothermometer. *Geochimica et Cosmochimica Acta*, **60**, 4285–4289.

Ding, Z. and Frost, R.L. (2002) Controlled rate thermal analysis of nontronite. *Thermochimica Acta*, **389**, 185–193.

Eguiluz, L., Fernández, J., Garrote, A., Liñán, E. and Quesada, C. (1984) Sucesiones estratigráficas del anticlinorio

Olivenza-Monesterio en la transversal Montemolín-Arroyomolinos. *Cuadernos Laboratorio Xeolóxico Laxe*, **8**, 117–123.

Frost, R.L. Kloprogge, J.T. and Ding, Z. (2002) Near-infrared spectroscopy study of nontronites and ferruginous smectites. *Spectrochimica Acta Part A – Molecular and Biomolecular Spectroscopy*, **58**, 1657–1668.

Gibbons, W. and Moreno, T. (2002) Introduction and overview. Pp. 1–6 in: *The Geology of Spain* (W. Gibbons and T. Moreno, editors). The Geological Society, London.

Godfrey, J.D. (1962) The deuterium content of hydrous minerals from the East Central Sierra Nevada and Yosemite National Park. *Geochimica et Cosmochimica Acta*, **26**, 1215–1245.

Goodman, B.A., Russell, J.D., Fraser, A.R. and Woodhams, F.W.D. (1976) A Mössbauer and IR spectroscopic study of the structure of nontronite. *Clays and Clay Minerals*, **24**, 53–59.

Güven, N. (1988) Smectites. Pp. 497–559 in: *Hydrous Phyllosilicates (Exclusive of Micas)* (S.W. Bailey, editor). Reviews in Mineralogy, **19**. Mineralogical Society of America, Washington, D.C.

Harder, H. (1976) Nontronite synthesis at low temperatures. *Chemical Geology*, **18**, 169–180.

Huang, W.H. and Keller, W.D. (1972) Geochemical mechanics for the dissolution, transport, and deposition of aluminium in the zone of weathering. *Clays and Clay Minerals*, **20**, 69–74.

IGME – Instituto Geológico y Minero de España (1988) *Memoria de la Hoja Geológica nº 804 (Oliva de Mérida) a escala 1:50,000.* 59 pp. Ministerio de Industria y Energía, Madrid.

Juniper, S.K. and Tebo, M. (1995) Microbe-metal interactions and mineral deposition at hydrothermal vents. Pp. 219–253 in: *The Microbiology of Deep-Sea Hydrothermal Vents* (D.M. Karl, editor). CRC Press, New York.

Keeling, J.L., Raven, M.D. and Gates, W.P. (2000) Geology and characterization of two hydrothermal nontronites from weathered metamorphic rocks at the Uley graphite mine, South Australia. *Clays and Clay Minerals*, **48**, 537–548.

Köhler, B., Singer, A. and Stoffers, P. (1994) Biogenic nontronite from marine white smoker chimneys. *Clays and Clay Minerals*, **42**, 689–701.

Köster, H.M., Ehrlicher, U., Gilg, H.A., Jordan, R., Murad, E. and Onnich, K. (1999) Mineralogical and chemical characteristics of five nontronites and Fe-rich smectites. *Clay Minerals*, **34**, 579–599.

Kyser, T.K. (1987) Equilibrium fractionation factors for stable isotopes. Pp. 1–84 in: *Stable Isotope Geochemistry of Low Temperature Fluids* (T.K. Kyser, editor). Short Course Handbook, **13**. Mineralogical Association of Canada, Toronto.

Mizutani, T., Fukushima, Y., Okada, A., Kamigaito, O. and Kobayashi, T. (1991) Synthesis of 1:1 and 2:1 iron phyllosilicates and characterization of their iron state by Mössbauer spectroscopy. *Clays and Clay Minerals*, **39**, 381–386.

Moore, D.M. and Reynolds, R.C. (1997) *X-ray Diffraction and the Identification and Analysis of Clay Minerals.* Oxford University Press, New York, 378 pp.

Murnane, R. and Clague, D.A. (1983) Nontronite from a low-temperature hydrothermal system on the Juan de Fuca Ridge. *Earth and Planetary Science Letters*, **65**, 343–352.

Nicholson, R.V. (1994) Iron-sulfide oxidation mechanisms: laboratory studies. Pp. 163–183 in: *The Environmental Geochemistry of Sulfide Mine-Wastes* (D.W. Blowes and J.L. Jambor, editors). Short Course Handbook, **22**. Mineralogical Association of Canada, Toronto.

Paktunc, A.D. (1999) Characterization of mine wastes for prediction of acid mine drainage. Pp. 19–40 in: *Environmental Impacts of Mining Activities* (J.M. Azcue, editor). Springer, Berlin.

Petit, S., Caillaud, J., Righi, D., Madejová, J., Elsass, F. and Köster, H.M. (2002) Characterization and crystal chemistry of an Fe-rich montmorillonite from Ölberg, Germany. *Clay Minerals*, **37**, 283–297.

Quesada, C. (1990) Precambrian successions in SW Iberia: their relationship to Cadomian orogenic events. Pp. 353–362 in: *The Cadomian Orogeny* (R.S. D'Lemos, R.A. Strachan and C.G. Topley, editors). Special Publication, **51**, Geological Society, London.

Reyes, A.G. and Read, S. (2002) Nontronite formation in rhyolitic ignimbrite. *Geochimica et Cosmochimica Acta*, **66** (15A), A635, Suppl. 1.

Russell, J.D. and Fraser, A.R. (1994) Infrared methods. Pp. 11–67 in: *Clay Mineralogy: Spectroscopic and Chemical Determinative Methods* (M.J. Wilson, editor). Chapman & Hall, London.

Savin, S.M. and Epstein, S. (1970) The oxygen and hydrogen isotope geochemistry of clay minerals. *Geochimica et Cosmochimica Acta*, **34**, 25–42.

Shenk, K. and Armbruster, T. (1985) Beidellite-nontronite, an alteration product of cordierite in the rhyolite from Torniella (Tuscany, Italy). *Neues Jahrbuch für Mineralogie Monatshefte*, **9**, 385–395.

Sheppard, S.M.F. and Gilg, H.A. (1996) Stable isotope geochemistry of clay minerals. *Clay Minerals*, **31**, 1–24.

Singer, A. and Stoffers, P. (1987) Mineralogy of a hydrothermal sequence in a core from the Atlantis II Deep, Red Sea. *Clay Minerals*, **22**, 251–267.

Singer, A., Stoffers, P., Heller-Kallai, L. and Szafranek, D. (1984) Nontronite in a deep-sea core from the South Pacific. *Clays and Clay Minerals*, **32**, 375–383.

Ueshima, M. and Tazaki, K. (2001) Possible role of microbial polysaccharides in nontronite formation. *Clays and Clay Minerals*, **49**, 292–299.

(*Received 27 January 2003; revised 13 August 2003; Ms. 755; A.E. Ray E. Ferrell*)